modelling

Article

The Data Assimilation Approach in a Multilayered Uncertainty Space

Martin Drieschner *, Clemens Herrmann and Yuri Petryna

Chair of Structural Mechanics, Technische Universität Berlin, Gustav-Meyer-Allee 25, 13355 Berlin, Germany; c.herrmann.1@tu-berlin.de (C.H.); yuriy.petryna@tu-berlin.de (Y.P.)
* Correspondence: martin.drieschner@tu-berlin.de

Abstract: The simultaneous consideration of a numerical model and of different observations can be achieved using data-assimilation methods. In this contribution, the ensemble Kalman filter (EnKF) is applied to obtain the system-state development and also an estimation of unknown model parameters. An extension of the Kalman filter used is presented for the case of uncertain model parameters, which should not or cannot be estimated due to a lack of necessary measurements. It is shown that incorrectly assumed probability density functions for present uncertainties adversely affect the model parameter to be estimated. Therefore, the problem is embedded in a multilayered uncertainty space consisting of the stochastic space, the interval space, and the fuzzy space. Then, we propose classifying all present uncertainties into aleatory and epistemic ones. Aleatorically uncertain parameters can be used directly within the EnKF without an increase in computational costs and without the necessity of additional methods for the output evaluation. Epistemically uncertain parameters cannot be integrated into the classical EnKF procedure, so a multilayered uncertainty space is defined, leading to inevitable higher computational costs. Various possibilities for uncertainty quantification based on probability and possibility theory are shown, and the influence on the results is analyzed in an academic example. Here, uncertainties in the initial conditions are of less importance compared to uncertainties in system parameters that continuously influence the system state and the model parameter estimation. Finally, the proposed extension using a multilayered uncertainty space is applied on a multi-degree-of-freedom (MDOF) laboratory structure: a beam made of stainless steel with synthetic data or real measured data of vertical accelerations. Young's modulus as a model parameter can be estimated in a reasonable range, independently of the measurement data generation.

Keywords: data assimilation; ensemble Kalman filter; aleatory and epistemic uncertainty; uncertainty quantification; stochastic variables; interval variables; fuzzy variables

check for updates

Citation: Drieschner, M.; Herrmann, C.; Petryna, Y. The Data Assimilation Approach in a Multilayered Uncertainty Space. *Modelling* **2023**, *4*, 529–547. https://doi.org/10.3390/modelling4040030

Academic Editor: Günther Meschke

Received: 27 September 2023
Revised: 1 November 2023
Accepted: 2 November 2023
Published: 8 November 2023

1. Introduction

Data assimilation is a widespread method that combines theory (usually in the form of a numerical model evaluation) with observations, e.g., measurement data of some model outputs, to optimally determine reasonable system states. The method is mainly known for weather and climate forecasts [1], but it has also applied been in various fields like robotics [2], economics [3], and many industrial branches [4] in recent decades.

In statistics, data assimilation can be considered as a Bayesian estimation problem based on the Bayes' theorem $P(H|D) = P(D|H)P(H)/P(D)$ with hypothesis H and data D. Basically, it is assumed that the numerical model and the observations are subject to uncertainty, so probability density functions are defined for the prior $P(H)$, the likelihood function $P(D|H)$, the model evidence $P(D)$, and the posterior $P(H|D)$. If normal distributions, represented using their mean and covariance, are used for modeling the uncertainty, Kalman filters can be applied. Kalman filters are used to continuously improve the results (system state) of time-discrete models involving observations (measurements). The standard Kalman filter [5] is efficient for low-dimensional problems and can process only linear systems. For nonlinear problems including a large number of variables, the ensemble Kalman filter (EnKF) [6,7], the ensemble square root filter (EnSRF) [8,9], the reduced rank square root Kalman filter (RRSQRT) [10,11], or the unscented Kalman filter (UKF) [12–14] are suitable choices. A comprehensive overview and a comparison of different Kalman filters can be found in [15,16].

In the case of uncertainties, e.g., in system parameters, robust Kalman filters have been developed in the past. The uncertainties can be quantified in different ways, e.g., with interval [17,18] or stochastic variables [19].

In addition to Kalman filters using probability distributions, a fuzzy Kalman filter based on possibility theory has been developed [20], improved [21] and applied on practical experiments [22] in recent years. Also, in the case of fuzzy Kalman filters, the robustness regarding additional uncertain system parameters have to be considered to obtain usable results.

In this contribution, diverse uncertainties in the initial conditions and/or system parameters are integrated into the data assimilation approach by using a multilayered uncertainty space. The numerical model is embedded in the uncertainty space in which uncertainties based on probability and the possibility theory can be defined simultaneously. Therefore, we propose classifying the present uncertainties into aleatory and epistemic ones [23]. Different quantification approaches are then compared using an academic example. Finally, the applicability of the general concept with a multilayered uncertainty space is shown on a MDOF laboratory structure.

The remainder of this paper is organized as follows: In Section 2, a brief introduction to Kalman filters is given. Then, the ensemble Kalman filter (EnKF) as the basis of this contribution is mathematically introduced, including the possibility of estimating model parameters simultaneously. Next, the basic concepts for quantifying aleatory and epistemic uncertainties are presented, leading to a multilayered and nested uncertainty space. Furthermore, the integration of the ensemble Kalman filter into the multilayered uncertainty space is formally developed. In Section 3, different possibilities for uncertainty quantification are shown in an academic example. In addition, an engineering application with synthetic or, respectively, with real measurement data is given to demonstrate the practical applicability of the proposed extensions. Finally, the discussion of the results and an outlook are given in Section 4.

2. Materials and Methods

After introducing the ensemble Kalman filter (EnKF) in Section 2.1, the basic concepts for aleatorically and epistemically uncertain parameters are given in Section 2.2. In Section 2.3, the proposal to embed the EnKF in a multilayered uncertainty space for taking both uncertainty types into account is formally presented.

2.1. The Ensemble Kalman Filter (EnKF)

In this contribution, the EnKF is used without loss of generality since other filters can also be incorporated into the general scheme in Section 2.3. The ensemble Kalman filter (EnKF) is a Monte Carlo implementation of the Bayesian estimation problem. It is applicable to various nonlinear problems [24,25]. The combined state and parameter estimation [26] or a multiplicative model parameter estimation [27] is also possible within the EnKF. With spatial heterogeneity of parameters in the underlying model, the use of a proper orthogonal-decomposition-based ensemble Kalman filter (POD-based EnKF) can efficiently reduce the problem dimension [28]. Generally speaking, EnKFs represent the distribution of the system state $\boldsymbol{x}$ by using an ensemble and replacing the covariance matrix with the sample covariance computed from the ensemble. An ensemble consists of q members and can be seen as a collection of system state vectors.

The bases are the (nonlinear) model equation and the measurement equation (linearized here):

$$\begin{aligned} \boldsymbol{x}_k &= f(\boldsymbol{x}_{k-1}, \boldsymbol{p}_{k-1}) + \boldsymbol{w}_{k-1} \qquad \text{and} \\ \boldsymbol{y}_k &= d(\boldsymbol{x}_k) + \boldsymbol{v}_{k-1} = \boldsymbol{D} \cdot \boldsymbol{x}_k + \boldsymbol{v}_{k-1} \end{aligned} \tag{1}$$

with

$$\begin{array}{rll} \text{system state vector} & \boldsymbol{x}_k \in \mathbb{R}^n & , \\ \text{system input vector} & \boldsymbol{p}_k \in \mathbb{R}^l & , \\ \text{system noise vector} & \boldsymbol{w}_k \in \mathbb{R}^n & , \\ \text{measurement vector} & \boldsymbol{y}_k \in \mathbb{R}^m & , \\ \text{mapping matrix} & \boldsymbol{D} \in \mathbb{R}^{m\times n} & \text{and} \\ \text{measurement noise vector} & \boldsymbol{v}_k \in \mathbb{R}^m & \end{array} \tag{2}$$

at the k-th time step. The uncertainty is quantified using the uncorrelated vectors $\boldsymbol{w}_k$ and $\boldsymbol{v}_k$ with underlying normal distributions representing white noise. All means are set to zero, and the scattering is quantified using a model noise matrix $\boldsymbol{Q}_k$ and a measurement noise matrix $\boldsymbol{R}_k$, respectively. Both matrices provide the possibility to trust the numerical model prediction or the observation more. This is taken into account within the correction step by the Kalman gain $\boldsymbol{K}_k$; see below.

2.1.1. Procedure

The procedure of the EnKF is depicted in Algorithm 1, consisting of

1. One-time initialization
2. Prediction or **f**orecast $\longrightarrow$ $\bullet^{\mathrm{f}}$
3. Correction or **a**nalysis $\longrightarrow$ $\bullet^{\mathrm{a}}$

Algorithm 1: EnKF procedure [29].

Initialization

Create an ensemble with q members representing the probability density function (PDF) of the initial state.

$$\boldsymbol{X}_0 = \left(\boldsymbol{x}_0^{\mathrm{a}_1}, \boldsymbol{x}_0^{\mathrm{a}_2}, \ldots, \boldsymbol{x}_0^{\mathrm{a}_q}\right), \quad \boldsymbol{X}_0 \in \mathbb{R}^{n\times q} \tag{3}$$

Forecast step

$$\boldsymbol{x}_k^{\mathrm{f}_i} = f\left(\boldsymbol{x}_{k-1}^{\mathrm{a}_i}, \boldsymbol{p}_{k-1}\right) + \boldsymbol{w}_{k-1}^i, \quad i = 1\ldots q \tag{4}$$

$$\bar{\boldsymbol{x}}_k^{\mathrm{f}} = \frac{1}{q}\sum_{i=1}^{q} \boldsymbol{x}_k^{\mathrm{f}_i} \tag{5}$$

Analysis step

$$\boldsymbol{y}_k^{\mathrm{f}_i} = \boldsymbol{D}\cdot\boldsymbol{x}_k^{\mathrm{f}_i}, \quad i = 1\ldots q \tag{6}$$

$$\bar{\boldsymbol{y}}_k^{\mathrm{f}} = \frac{1}{q}\sum_{i=1}^{q} \boldsymbol{y}_k^{\mathrm{f}_i} \tag{7}$$

$$\boldsymbol{P}_{xy,k} = \frac{1}{q-1}\sum_{i=1}^{q}\left(\boldsymbol{x}_k^{\mathrm{f}_i} - \bar{\boldsymbol{x}}_k^{\mathrm{f}}\right)\cdot\left(\boldsymbol{y}_k^{\mathrm{f}_i} - \bar{\boldsymbol{y}}_k^{\mathrm{f}}\right)^{\mathrm{T}} \tag{8}$$

$$\boldsymbol{P}_{yy,k} = \frac{1}{q-1}\sum_{i=1}^{q}\left(\boldsymbol{y}_k^{\mathrm{f}_i} - \bar{\boldsymbol{y}}_k^{\mathrm{f}}\right)\cdot\left(\boldsymbol{y}_k^{\mathrm{f}_i} - \bar{\boldsymbol{y}}_k^{\mathrm{f}}\right)^{\mathrm{T}} + \boldsymbol{R}_k \tag{9}$$

$$\boldsymbol{K}_k = \boldsymbol{P}_{xy,k}\cdot\left(\boldsymbol{P}_{yy,k}\right)^{-1} \tag{10}$$

$$\boldsymbol{x}_k^{\mathrm{a}_i} = \boldsymbol{x}_k^{\mathrm{f}_i} + \boldsymbol{K}_k\cdot\left(\boldsymbol{y}_k + \boldsymbol{v}_k^i - \boldsymbol{y}_k^{\mathrm{f}_i}\right), \quad i = 1\ldots q \tag{11}$$

$$\bar{\boldsymbol{x}}_k^{\mathrm{a}} = \frac{1}{q}\sum_{i=1}^{q} \boldsymbol{x}_k^{\mathrm{a}_i} \tag{12}$$

The matrices $\boldsymbol{P}_{xy,k}$ and $\boldsymbol{P}_{yy,k}$ in Equations (8) and (9) contain the error covariance matrix of the state $\boldsymbol{P}_k \in \mathbb{R}^{n\times n}$, well-known from the KF algorithms:

$$\begin{array}{rcll} \boldsymbol{P}_{xy,k} & = & \boldsymbol{P}_k\cdot\boldsymbol{D}^{\mathrm{T}} & \text{and} \\ \boldsymbol{P}_{yy,k} & = & \boldsymbol{D}\cdot\boldsymbol{P}_k\cdot\boldsymbol{D}^{\mathrm{T}} + \boldsymbol{R}_k\,. & \end{array} \tag{13}$$

Note that the EnKF needs "perturbed observations", which are achieved by $\boldsymbol{v}_k^i$ in Equation (11) in order to not underestimate the error covariance matrix.

2.1.2. Estimation of Model Parameters

The EnKF can also be used to estimate model parameters simultaneously with the prediction of the system state. For this purpose, the original state $\boldsymbol{x}$ must be extended by the parameters $\boldsymbol{b}$ to be estimated. This results in an augmented state vector $\boldsymbol{z} = (\boldsymbol{x}, \boldsymbol{b})^{\mathrm{T}}$, which can be used analogously to $\boldsymbol{x}$ in the above procedure. The development of the model parameters $\boldsymbol{b}_k^{\mathrm{f}_i} = (1-\beta)\boldsymbol{b}_{k-1}^{\mathrm{a}_i} + \beta \boldsymbol{b}_{k-1}^{\mathrm{f}_i}$ can be defined with a scalar value $\beta \in [0,1]$ in order to prevent the model from diverging [27]. Analogous to Equation (4), a noise vector $\boldsymbol{w}_{\boldsymbol{b}_k}$ is also added to the unknown model parameters for additional scatter. Note that only the number of model parameters that can be estimated as independent measurements are available.

2.2. Aleatory and Epistemic Uncertainties

Various additional uncertainties $\boldsymbol{c}$ can be present in the system, which have to be considered in the numerical simulations. Material properties, geometrical dimensions, and also boundary conditions can be uncertain, influencing the prediction of the system state $\boldsymbol{x}_k$ and the estimation of unknown model parameters $\boldsymbol{b}_k$. Uncertain parameters can be divided into two groups [23], aleatory uncertainties $\boldsymbol{c}_{\mathrm{alea}}$ and epistemic uncertainties $\boldsymbol{c}_{\mathrm{epis}}$, with $\boldsymbol{c} = \boldsymbol{c}_{\mathrm{alea}} \cup \boldsymbol{c}_{\mathrm{epis}}$ and $\boldsymbol{c}_{\mathrm{alea}} \cap \boldsymbol{c}_{\mathrm{epis}} = \emptyset$.

Aleatory uncertainties $\boldsymbol{c}_{\mathrm{alea}}$ are caused by randomness and natural variability and are therefore also referred to as irreducible uncertainties. Statistical information with a sufficient amount of realizations is at our disposal to reliably model and quantify the uncertainty via a random variable X. The underlying distribution can be expressed by the probability density function (PDF) $f_X(x, \boldsymbol{\lambda})$ or the cumulative distribution function (CDF) $F_X(x, \boldsymbol{\lambda})$, where $\boldsymbol{\lambda}$ is the vector of shape parameters of the underlying PDF. The PDF and CDF of X are related via the integral

$$F_X(x) = \int_{-\infty}^{x} f_X(t)\mathrm{d}t\,. \tag{14}$$

In this study, normal distributions $\mathcal{N}(\mu, \sigma^2)$ with μ as the mean value and σ^2 as variance or lognormal distributions $\mathcal{LN}(\mu, \sigma^2)$ with μ as the mean value of logarithmic values and σ^2 as variance of logarithmic values are used for all random variables; see Figure 1 (top left/top right).

Epistemic uncertain parameters $\boldsymbol{c}_{\mathrm{epis}}$ are based on a limited number of data, subjectivity, or expert knowledge, and no statistical information is given that could reduce the uncertainty. These uncertainties can be modeled using non-stochastic variables [30], e.g., as interval $\bar{x}$ or as fuzzy set $\tilde{x}$. An interval $\bar{x}$ is defined by a lower and upper bound

$$\bar{x} = [a, b]\,, \tag{15}$$

whereas a fuzzy set $\tilde{x}$ is expressed using its membership function

$$\tilde{x} = \{(x, \mu_{\tilde{x}}(x) \in [0,1])\}\,. \tag{16}$$

Note that an interval is a special case of a fuzzy set with a membership function value of either $\mu_{\tilde{x}} = 1$ (total membership) or $\mu_{\tilde{x}} = 0$ (non-membership). In this study, interval variables or fuzzy variables with a triangular membership function, called triangular fuzzy numbers TFN$\langle a, b, c\rangle$, with support $[a, c]$ and core value b, are used for epistemic uncertain parameters $\boldsymbol{c}_{\mathrm{epis}}$; see Figure 1 (bottom left/bottom right) [31].

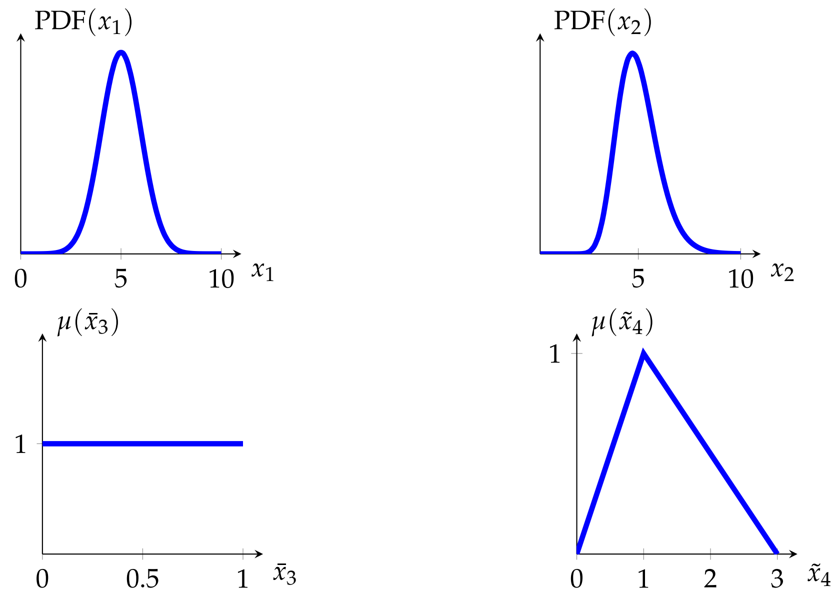

Figure 1. Applied uncertainty models: (**top left**): normal distribution $x_1 \sim \mathcal{N}(\mu, \sigma^2) = \mathcal{N}(5, 1)$, (**top right**): lognormal distribution $x_2 \sim \mathcal{LN}(\mu, \sigma^2) = \mathcal{LN}(5, 1)$, (**bottom left**): interval $\bar{x}_3 = [a, b] = [0, 1]$, (**bottom right**): triangular fuzzy number $\tilde{x}_4 = \mathrm{TFN}\langle a, b, c\rangle = \mathrm{TFN}\langle 0, 1, 3\rangle$.

Defining different uncertainty models simultaneously leads to a multilayered uncertainty space; see Figure 2. The deterministic finite element model (D) or an appropriate surrogate model ($\tilde{\mathrm{D}}$) is embedded in the uncertainty space, which generally consists of the stochastic space (S), the interval space (I), and the fuzzy space (F). Sometimes, some individual uncertainty spaces are empty and do not have to be considered. The simulation can then be simplified to the non-empty uncertainty spaces. The stochastic space is usually embedded in the interval space, which is itself embedded in the fuzzy space, leading to a nested analysis. The computational costs for the nested simulation can be calculated as $t_{\mathrm{tot}} = n_{\mathrm{tot}} \cdot t_{\mathrm{D}} = \sum_{i_{\mathrm{F}}=1}^{n_{\mathrm{F}}} \sum_{i_{\mathrm{I}}=1}^{n_{\mathrm{I}}(i_{\mathrm{F}})} \sum_{i_{\mathrm{S}}=1}^{n_{\mathrm{S}}(i_{\mathrm{I}}, i_{\mathrm{F}})} t_{\mathrm{D}}(i_{\mathrm{F}}, i_{\mathrm{I}}, i_{\mathrm{S}})$, with the number of samples in the fuzzy space n_{F}, the number of samples in the interval space n_{I} on the i_{F}-th fuzzy point, the number of samples in the stochastic space n_{S} on the i_{I}-th interval point, and the duration t_{D} of a single model evaluation. This approach of different uncertainty models leads to a polymorphic uncertainty modeling [30,32–34], for which different solution methods for the uncertainty propagation and evaluation methods for the assessment have to be applied. The framework `PolyUQ` [35] has been developed in `MATLAB` for those issues. The output, denominated as augmented state vector $\boldsymbol{z}_k(\boldsymbol{c})$ in Section 2.1.2, is in general influenced by the uncertain parameters $\boldsymbol{c}$; see Section 2.3 in detail.

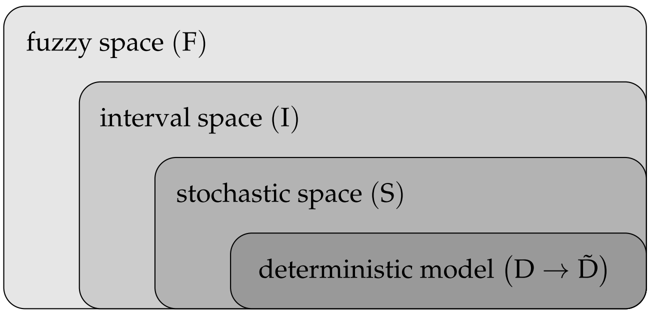

Figure 2. General scheme of a nested fuzzy-interval stochastic analysis.

2.3. *The Ensemble Kalman Filter (EnKF) in a Multilayered Uncertainty Space*

In this Section, the ensemble Kalman filter (EnKF) of Section 2.1 is integrated into the multilayered uncertainty space presented in Section 2.2. Since normally distributed random variables are used for the noise in the Kalman filter in this contribution, the EnKF is integrated directly into the stochastic space (S); see Figure 3.

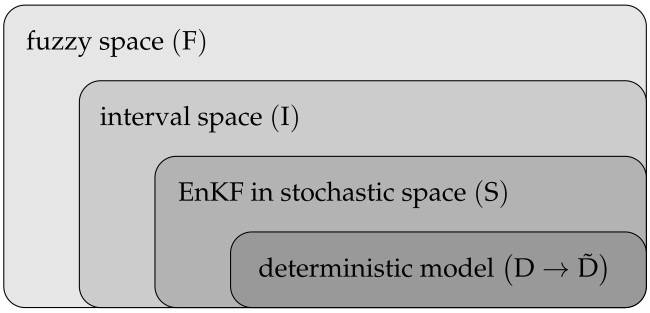

Figure 3. The EnKF embedded in the multilayered uncertainty space.

First, uncertain model parameters are distinguished in parameters $\boldsymbol{b}$ to be estimated and parameters $\boldsymbol{c}$ not to be estimated within the EnKF. The parameters $\boldsymbol{c}$ are classified as aleatorically ($\boldsymbol{c}_{\mathrm{alea}}$) or epistemically ($\boldsymbol{c}_{\mathrm{epis}}$) uncertain, and different uncertainty models can be applied. The output, namely the augmented state vector $\boldsymbol{z}_k(\boldsymbol{c}) = (\boldsymbol{x}_k(\boldsymbol{c}), \boldsymbol{b}_k(\boldsymbol{c}))^{\mathrm{T}}$, generally depends on all uncertain parameters $\boldsymbol{c} = \boldsymbol{c}_{\mathrm{alea}} \cup \boldsymbol{c}_{\mathrm{epis}}$.

Samples from $\boldsymbol{c}_{\mathrm{alea}}$ are used directly in the stochastic space within the EnKF without additional computational costs compared to the classical EnKF in Section 2.1. The output $\boldsymbol{z}_k$ remains a purely stochastic vector if only aleatory uncertain parameters $\boldsymbol{c}_{\mathrm{alea}}$ are given. The calculation of, e.g., the mean value or the standard deviation is then still possible without further methods.

Otherwise, the present epistemic uncertain parameters $\boldsymbol{c}_{\mathrm{epis}}$ cannot be integrated directly in the EnKF procedure. Additional methods are necessary, and additional computational costs are inevitable to take them into account. The EnKF is now executed for each sample from $\boldsymbol{c}_{\mathrm{epis}}$, since the interval and/or the fuzzy space are/is non-empty. Note that the used uncertainty models influence whether an uncertainty space is empty or not. Consequently, the output $\boldsymbol{z}_k(\boldsymbol{c}_{\mathrm{epis}})$ is defined in the multilayered uncertainty space. For the output interpretation, the nested structure has to be considered. The stochastic space is evaluated first, e.g., by determining the mean value on each sample of $\boldsymbol{c}_{\mathrm{epis}}$. In the next step, the non-empty interval space has to be evaluated, e.g., by determining the bounds of the output variables on each fuzzy sample of $\boldsymbol{c}_{\mathrm{epis}}$. Finally, the non-empty fuzzy space is considered. The membership function and also a defuzzified value for each time step k can be determined.

3. Results

The presented EnKF in the multilayered uncertainty space is applied to an academic example in Section 3.1 and on a laboratory structure in Section 3.2.

3.1. Academic Example

Below, an academic example is used to demonstrate the influence of various uncertainty models for aleatory and epistemic uncertainties on the augmented state vector $\boldsymbol{z}_k(\boldsymbol{c})$. The deterministic model (D) is an unloaded cantilever beam with longitudinal time-dependent degrees of freedom for the displacement $u(t)$, for the velocity $\dot{u}(t)$, and for the acceleration $\ddot{u}(t)$ at the end of the beam; see Figure 4. Young's modulus E, the cross-sectional area A, the density 2.454ρ, the damping ratio ξ, and the length L are (potentially uncertain) system parameters. The mass m of the equivalent single-degree-of-freedom system for the cantilever beam is then $m = 0.4075 \cdot 2.454\rho AL = \rho AL$. Note that the initial displacement $u_0 = u(0)$ and the initial velocity $\dot{u}_0 = \dot{u}(0)$ can be uncertain as well.

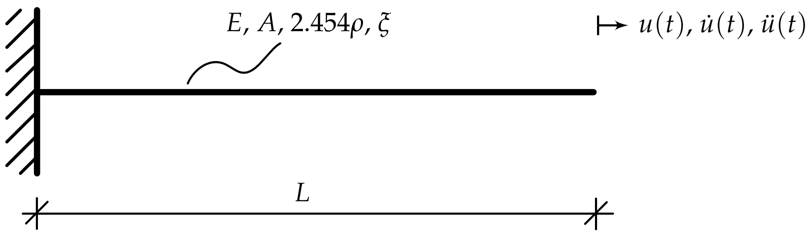

Figure 4. Cantilever beam as a deterministic model (D).

The underlying ordinary differential equation for the displacement $u(t)$ is given as $m\ddot{u}(t) + c\dot{u}(t) + ku(t) = 0$ with mass $m = \rho AL$, stiffness $k = EA/L$, damping $c = 2\xi\sqrt{km}$ and initial conditions u_0 and $\dot{u}_0$. A time-discrete solution with time steps $k = \{0, 1, \ldots, k_{\max}\}$ and time increment Δt can be achieved by using the Newmark method [36]. Alternatively, Equation (1) can be transformed into the following discrete formulation (for the unloaded case):

$$\begin{aligned} \mathbb{R}^n \ni \boldsymbol{x}_k &= \boldsymbol{A}_{\mathrm{dis}} \cdot \boldsymbol{x}_{k-1} + \boldsymbol{w}_{k-1} \quad \text{and} \\ \mathbb{R}^m \ni y_k &= u_k + v_{k-1} \end{aligned} \tag{17}$$

with $n = 2$, including displacement and velocity, and $m = 1$ for the displacement measurement (excluding velocity measurements for simplicity). The system transition matrix $\boldsymbol{A}_{\mathrm{dis}}$ can be derived using the state space representation:

$$\begin{aligned} \boldsymbol{A}_{\mathrm{dis}} &= \mathrm{e}^{\boldsymbol{A}\Delta t} \quad \text{with} \\ \boldsymbol{A} &= \begin{pmatrix} 0 & 1 \\ -\frac{E}{\rho L^2} & -2\xi\sqrt{\frac{E}{\rho L^2}} \end{pmatrix}. \end{aligned} \tag{18}$$

Note that the numerical prediction is independent of the cross-sectional area A, since the stiffness k and the mass m are both linearly dependent on A.

The quasi-continuous system state vector $\boldsymbol{x}(t) = (u(t), \dot{u}(t))^{\mathrm{T}}$ can finally be composed using the discrete solutions $\boldsymbol{x}_k = (u_k, \dot{u}_k)^{\mathrm{T}}$ on all time steps $k = \{0, 1, \ldots, k_{\max}\}$. Additionally, unknown model parameters $\boldsymbol{b}$ can be estimated in time within the EnKF by using the augmented state vector $\boldsymbol{z} = (\boldsymbol{x}, \boldsymbol{b})^{\mathrm{T}}$. Here, Young's modulus E has to be estimated. The initial Young's modulus E_0 is set to be a normally distributed random variable

$$E_0 \left[\mathrm{MN/m^2}\right] \sim \mathcal{N}\left(\mu_{E_0}, \sigma^2_{E_0}\right) = \mathcal{N}\left(0.5, (0.10 \cdot 0.5)^2\right) \tag{19}$$

with initial mean value μ_{E_0} and initial variance $\sigma^2_{E_0}$. The following normal distributions have been defined for the noise terms $\boldsymbol{w}_k$, v_k and $w_{E,k}$:

$$\begin{aligned} \boldsymbol{w}_k = \begin{pmatrix} w_{u_k} \\ w_{\dot{u}_k} \end{pmatrix} &\sim \begin{pmatrix} \mathcal{N}\left(0, \left(0.01 \cdot \mu_{u_k}\right)^2\right) \\ \mathcal{N}\left(0, \left(0.01 \cdot \mu_{\dot{u}_k}\right)^2\right) \end{pmatrix} \quad , \\ v_k &\sim \mathcal{N}\left(0, 0.005^2\right) \quad \text{and} \\ w_{E_k} &\sim \mathcal{N}\left(0, \left(0.001 \cdot \mu_{E_k}\right)^2\right). \end{aligned} \tag{20}$$

As the basis for all calculations, the values

$$\begin{aligned} E_{\mathrm{real}} &= 1\,\mathrm{MN/m^2} \quad , \\ A_{\mathrm{real}} &= 0.01\,\mathrm{m^2} \quad , \\ \rho_{\mathrm{real}} &= 1000\,\mathrm{kg/m^3} \quad , \\ \xi_{\mathrm{real}} &= 10\,\% \quad , \\ L_{\mathrm{real}} &= 1\,\mathrm{m} \quad , \\ u_{0,\mathrm{real}} &= 0.1\,\mathrm{m} \quad \text{and} \\ \dot{u}_{0,\mathrm{real}} &= 0.1\,\mathrm{m/s} \end{aligned} \tag{21}$$

are taken as real, and the initial state is quantified by

$$\begin{aligned} u_0 &\sim \mathcal{N}\left(\mu_{u_0}, \sigma_{u_0}^2\right) = \mathcal{N}\left(u_{0,\mathrm{real}}, (0.10 \cdot u_{0,\mathrm{real}})^2\right) \quad \text{and} \\ \dot{u}_0 &\sim \mathcal{N}\left(\mu_{\dot{u}_0}, \sigma_{\dot{u}_0}^2\right) = \mathcal{N}\left(\dot{u}_{0,\mathrm{real}}, (0.10 \cdot \dot{u}_{0,\mathrm{real}})^2\right) \end{aligned} \tag{22}$$

in the following unless otherwise specified.

The presented academic example is applied to different scenarios. The ensemble size is set to $q = 100$ at all time steps $k = \{0, 1, \ldots, 1000\}$. In Section 3.1.1, different uncertainty models for the uncertain initial conditions u_0 and $\dot{u}_0$ are defined, and the influence on the system state prediction as well as on the model parameter estimation is investigated. Aleatory and epistemic uncertainties in different model parameters are analyzed in Section 3.1.2. The monotonic behavior of the augmented state vector $\boldsymbol{z} = (\boldsymbol{x}, \boldsymbol{b})^{\mathrm{T}}$ can be presumed regarding Equation (18). This fact leads to an exact evaluation of the interval and the fuzzy space by using the vertex method [37] and the reduced transformation method [31], respectively. In the fuzzy space, eleven equidistantly distributed α-levels from 0.0 to 1.0 are used. The framework `PolyUQ` [35] is used for the numerical model evaluation, with different uncertainty models simultaneously present.

3.1.1. Uncertain Initial Conditions (u_0 and $\dot{u}_0$)

First, the initial conditions are defined as normally distributed random variables

$$\begin{aligned} u_0\,[\mathrm{m}] &\sim \mathcal{N}\left(0.12, 0.012^2\right) \quad \text{and} \\ \dot{u}_0\,[\mathrm{m/s}] &\sim \mathcal{N}\left(0.08, 0.008^2\right) \end{aligned} \tag{23}$$

with mean values $\mu_{u_0} = 0.12\,\mathrm{m} \neq 0.1\,\mathrm{m} = u_{0,\mathrm{real}}$ and $\mu_{\dot{u}_0} = 0.08\,\mathrm{m/s} \neq 0.1\,\mathrm{m/s} = \dot{u}_{0,\mathrm{real}}$. Within the classical EnKF procedure, a sample of the initial state is used, as shown in Equation (3), leading to the system state prediction and the model parameter estimation depicted in Figure 5.

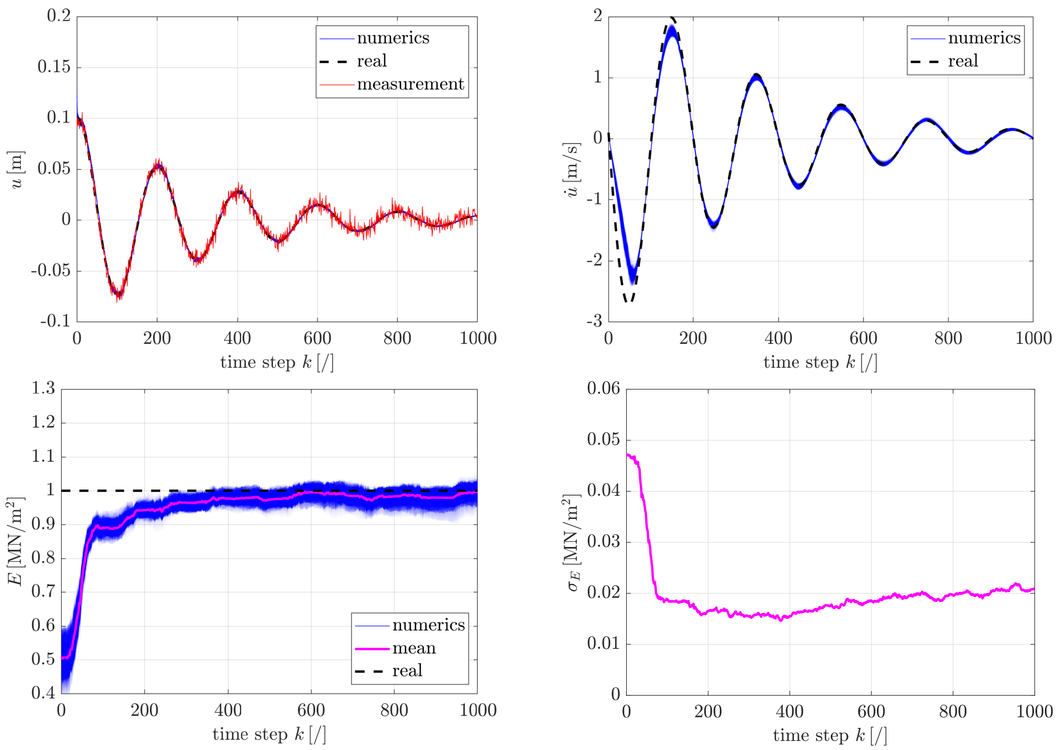

Figure 5. Results with stochastic initial conditions: (**top left**): displacement $u(t)$; (**top right**): velocity $\dot{u}(t)$; (**bottom left**): Young's modulus $E(t)$; (**bottom right**): standard deviation of Young's modulus $\sigma_E(t)$.

The prediction of the system state vector $\boldsymbol{x}(t) = (u(t), \dot{u}(t))^{\mathrm{T}}$ is practically exact, except for deviations at the beginning resulting from incorrect and scattering initial conditions. Despite the initial Young's modulus with a mean value of $\mu_{E_0} = 0.5\,\mathrm{MN/m^2}$, which is half the real value $E_{\mathrm{real}} = 1\,\mathrm{MN/m^2}$, Young's modulus $E(t)$ converges quickly to the real value with a coefficient of variation of around 2 %. The scattering is small, resulting from the random initial conditions.

It is also possible to define the initial conditions as epistemic uncertainties leading to non-stochastic uncertainty models, e.g., the mean values as the intervals

$$\begin{aligned} \mu_{u_0}\,[\mathrm{m}] &= [0.0829, 0.1571] \quad \text{and} \\ \mu_{\dot{u}_0}\,[\mathrm{m/s}] &= [0.0553, 0.1047] \end{aligned} \tag{24}$$

with a coefficient of variation of 10 %. The interval-stochastic results are displayed in Figure 6. Additionally, the real values, the measurements (if present), and the results from the classical EnKF procedure for Young's modulus are shown.

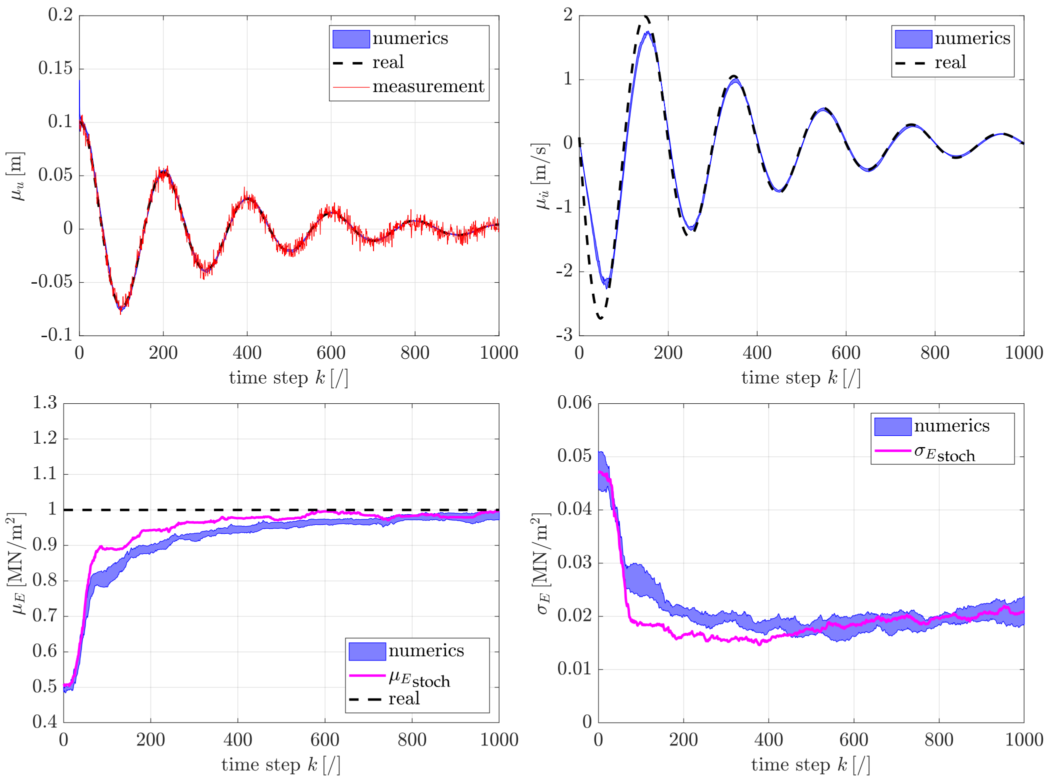

Figure 6. Results with interval-stochastic initial conditions: (**top left**): mean of displacement $\mu_u(t)$, (**top right**): mean of velocity $\mu_{\dot{u}}(t)$, (**bottom left**): mean of Young's modulus $\mu_E(t)$ compared to μ_E of Figure 5 (bottom left), (**bottom right**): standard deviation of Young's modulus $\sigma_E(t)$ compared to σ_E of Figure 5 (bottom right).

It can be concluded that the extension using other uncertainty models for the initial conditions does not have a concrete benefit in this example. The computational costs have been increased without a concrete change in the results. The system state vector is predicted again practically exactly, except for the values at the beginning. It is worth mentioning that models exist that are more sensitive to the initial conditions. In those cases, different uncertainty models would affect the system state prediction and the model parameter estimation much more.

3.1.2. Uncertain Model Parameters (L and ρ)

In this section, various model parameters are defined as uncertain using the different uncertainty models from Section 2.2. The effect on the augmented state vector $\boldsymbol{z}$ is investigated each time.

Stochastic problem: uncertain beam length L

In a purely stochastic problem, the beam length is defined as a lognormally distributed random variable

$$L\,[\mathrm{m}] \sim \mathcal{LN}\left(1, 0.1^2\right). \tag{25}$$

The mean value of logarithmic values μ_L is set to the real value L_{real}, and the standard deviation of logarithmic values σ_L is set to 0.1 m. For each of the q members within the ensemble, a sample of L is used, leading to the results shown in Figure 7.

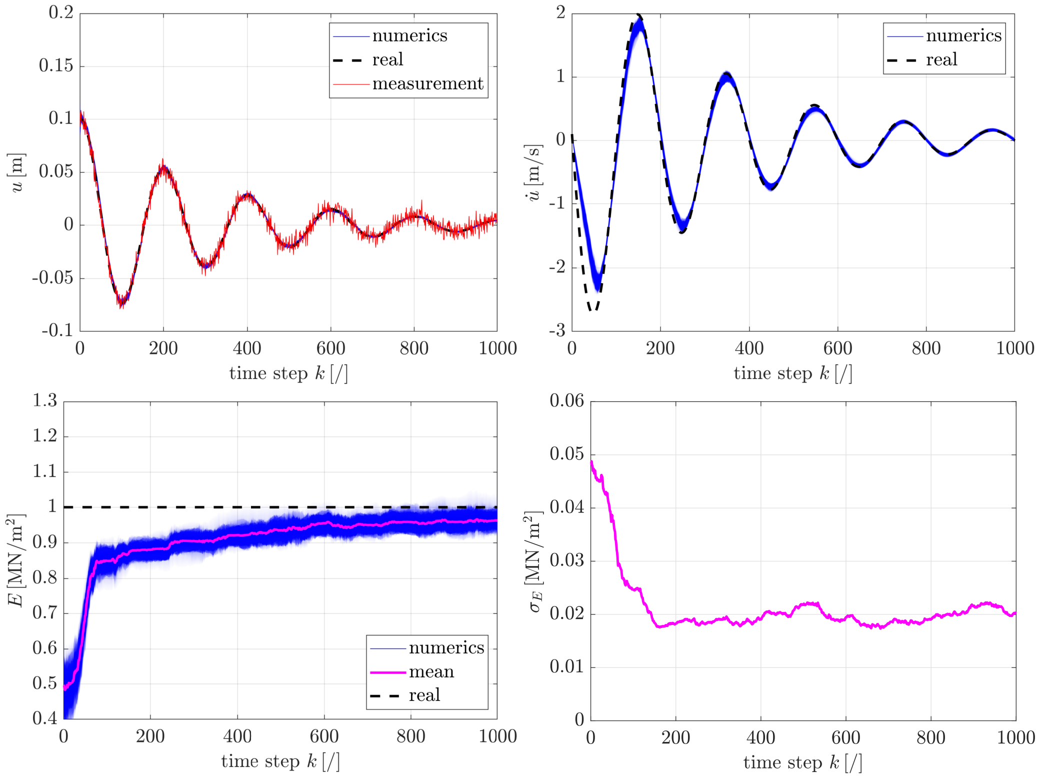

Figure 7. Results with stochastic beam length L: (**top left**): displacement $u(t)$; (**top right**): velocity $\dot{u}(t)$; (**bottom left**): Young's modulus $E(t)$; (**bottom right**): standard deviation of Young's modulus $\sigma_E(t)$.

It is obvious that the displacement and the velocity are predicted again quite perfectly, but the deviation of the mean value μ_E from the real value E_{real} is around 5 %. This results from the right-skewed distribution of L and the relation to E; see Equation (18). The model-parameter estimation depends (more or less) on the assumptions of other model parameters. Since the real values are in general unknown, a parameter study has been conducted with varying σ_L or μ_L; see Figure 8.

The best estimation of Young's modulus can be achieved naturally by having no scattering and the correct mean value $\mu_L = \mu_{\mathrm{real}}$; see the blue curve in Figure 8 (left). A variation in one of both values leads to bad or useless estimations. If exact values are unknown, it should be avoided to assume a pdf, but it can be useful to apply other non-stochastic uncertainty models.

Interval-stochastic problem: uncertain density $\bar{\rho}$

In this section, the density ρ is assumed to be uncertain using the interval

$$\bar{\rho}\left[\mathrm{kg}/\mathrm{m}^3\right] = [900, 1200] \tag{26}$$

around the real value $\rho_{\mathrm{real}} = 1000\,\mathrm{kg}/\mathrm{m}^3$. As in the previous examples, the system state vector $\boldsymbol{x}$ is predicted practically exactly. A value E is determined to an "associated" value ρ in each time step k. Since the density is now defined as an interval variable, the mean and the standard deviation of Young's modulus are now also intervals; see Figure 9.

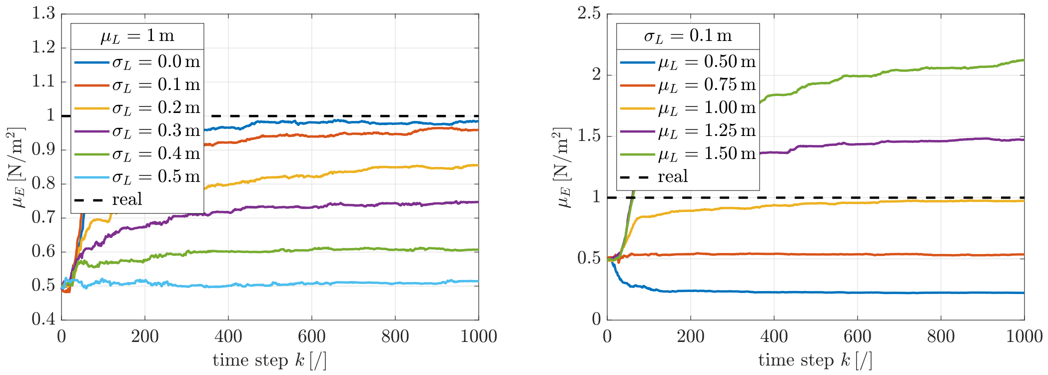

Figure 8. Parameter study within the stochastic problem: (**left**): varying σ_L [m] values for fixed $\mu_L = 1\,\mathrm{m}$, (**right**): varying μ_L [m] values for fixed $\sigma_L = 0.1\,\mathrm{m}$.

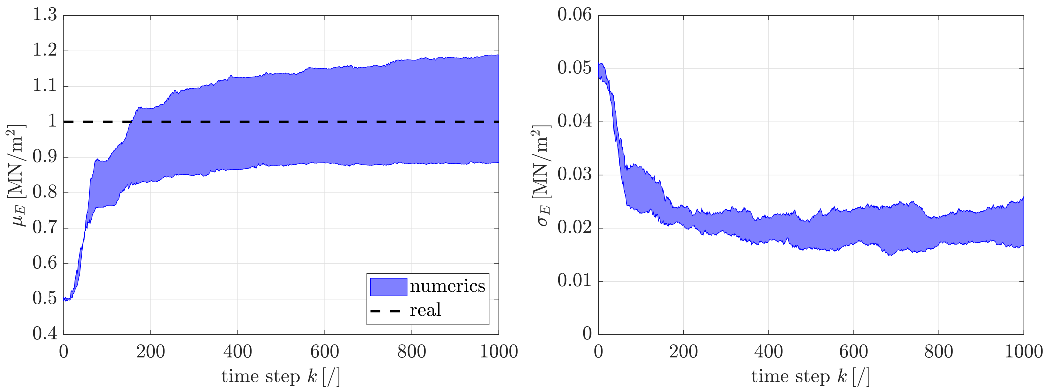

Figure 9. Results with interval-valued density $\bar{\rho}$: (**left**): mean of Young's modulus $\mu_E(t)$, (**right**): standard deviation of Young's modulus $\sigma_E(t)$.

The real value of Young's modulus E_{real} is inside the bounds of the predicted interval-valued mean μ_E, except for the first time steps. The interval-valued standard deviation σ_E also remains small with a maximum of around $0.026\,\mathrm{MN}/\mathrm{m}^2$ at the final time step. If more data about the uncertain density $\bar{\rho}$ were available, the epistemic uncertainty could be reduced, leading to a smaller range of possible values for Young's modulus E. In the next Section, the interval-based idea is extended by defining a fuzzy-valued density $\tilde{\rho}$.

Fuzzy-stochastic problem: uncertain density $\tilde{\rho}$

The extension from intervals to fuzzy values is shown by defining the density $\tilde{\rho}$ as a triangular fuzzy number:

$$\tilde{\rho}\left[\mathrm{kg}/\mathrm{m}^3\right] = \mathrm{TFN}\langle 900, 1000, 1200\rangle\,. \tag{27}$$

The real value ρ_{real} is assumed on the core of the fuzzy variable. If an interval is preferred on the core, a trapezoidal fuzzy interval [31,35] can be used instead. The extension to Figure 9 is given in Figure 10.

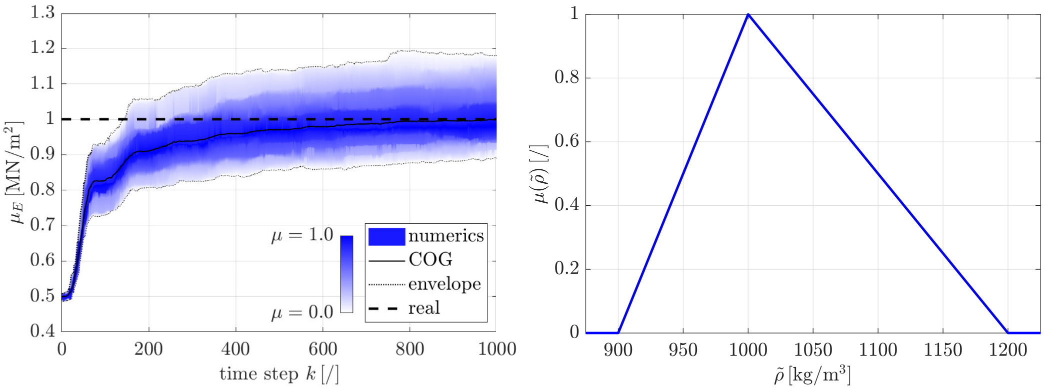

Figure 10. Results with fuzzy-valued density $\tilde{\rho}$: (**left**): mean of Young's modulus $\mu_E(t)$, (**right**): fuzzy-valued density $\tilde{\rho}$.

The envelope in Figure 10 (left) is equivalent to the solution in Figure 9 (left) since the support is defined with the same bounds as the interval in Equation (26). Decreasing the uncertainty leads to a higher membership function value in Figure 10 (right) with the exact value for $\mu = 1.0$. As a consequence, the blue shading in Figure 10 (left) is darker for higher membership-function values around the real value E_{real}. Finally, the membership function has been defuzzified [38] at each time step k, leading to a scalar value, here namely the center of gravity (COG). The COG curve is also in good agreement with the real value.

Finally, it should be mentioned that it is possible to combine different uncertainty models for the same parameter, obtaining, for example, a random variable with interval-valued parameters $\bar{\boldsymbol{\lambda}}$. Furthermore, interval and fuzzy variables can be simultaneously present in the same problem. These aspects can be found, for example, in [35] but are beyond the scope of the present paper.

3.2. Laboratory Structure

In this section, a beam made of stainless steel with synthetic or real measurement data of vertical accelerations is investigated. The beam has a length of $L = 4.0\,\text{m}$ between two supports with 0.20 m lateral overhangs on each side. The cross section is a box girder with an outer width of $w = 0.05\,\text{m}$, an outer height of $h = 0.03\,\text{m}$, and a wall thickness of $t = 0.0026\,\text{m}$, leading to a cross-sectional area $A = 3.89 \cdot 10^{-4}\,\text{m}^2$ and moments of inertia $I_y = 5.56 \cdot 10^{-8}\,\text{m}^4$ and $I_z = 1.27 \cdot 10^{-7}\,\text{m}^4$. The material is assumed to be homogeneous with a density of $\rho = 8000\,\text{kg/m}^3$. Isotropic behavior is defined via a Young's modulus value that is to be estimated with initial mean value μ_{E_0} = 100,000 MN/m^2 and initial standard deviation σ_{E_0} = 10,000 MN/m^2 and a Poisson's ratio of $\nu = 0.3$. For the damping ratio, a triangular fuzzy number $\tilde{\xi}\,[\%] = \text{TFN}\langle 0.00, 0.50, 1.00\rangle$ is defined. Additional overhangs with a length of $l_{\text{add}} = 0.125\,\text{m}$ have been welded in the beam center on both sides for various measurement procedures. The additional mass of $m_{\text{add}} = 0.907\,\text{kg}$ is taken into account in the numerical model.

The numerical finite element model is defined in the x-y-plane and consists of 21 nodes, each one with three degrees of freedom (u_x, u_y, ϕ_z), leading to 63 system degrees of freedom in total. The origin of the x-y coordinate system is located in the left support; see Figure 11 (top). Consequently, the translational degrees of freedom u_x and u_y are fixed at $x = 0\,\text{m}$ and $x = 4\,\text{m}$. A free vibration test ($\boldsymbol{p} = \boldsymbol{p}_{\text{own}}$, $\forall t$) is defined with the following initial conditions:

$$\begin{aligned} \boldsymbol{u}_0 &= \boldsymbol{K}^{-1} \cdot (\boldsymbol{p}_{\text{own}} + \boldsymbol{p}_{\text{add}}) &&, \\ \dot{\boldsymbol{u}}_0 &= \boldsymbol{0} && \text{and} \\ \ddot{\boldsymbol{u}}_0 &= \boldsymbol{M}^{-1} \cdot (\boldsymbol{p}_0 - \boldsymbol{C} \cdot \dot{\boldsymbol{u}}_0 - \boldsymbol{K} \cdot \boldsymbol{u}_0)) = -\boldsymbol{M}^{-1} \cdot \boldsymbol{p}_{\text{add}} && \end{aligned} \tag{28}$$

with $\boldsymbol{M}$, $\boldsymbol{C}$, and $\boldsymbol{K}$ indicating the mass, damping, and stiffness matrices, respectively.

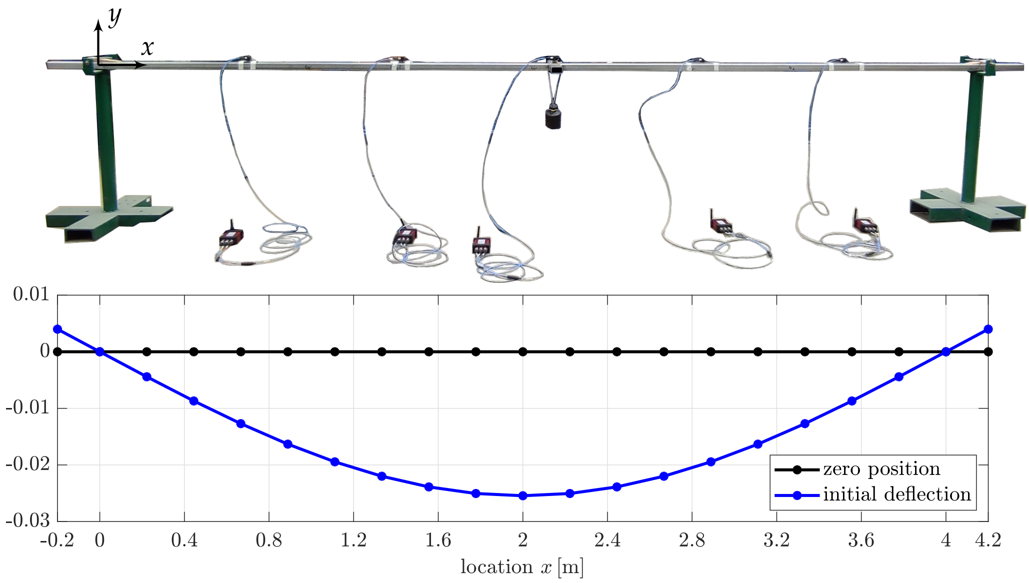

Figure 11. Beam made of stainless steel with initial deflection $\boldsymbol{u}_{0,y}$ [m] due to dead load and additional mass of 2 kg in the beam center: (**top**): real structure with five accelerometers, (**bottom**): calculated deflection of the beam with E = 100,000 MN/m^2.

The initial displacement $\boldsymbol{u}_0$ results from the dead load of the beam ($\boldsymbol{p}_{\text{own}}$) and an additional mass of 2 kg in the beam center ($\boldsymbol{p}_{\text{add}}$); see Figure 11 (top). Note that the additional mass is only present at the beginning and not during the free vibration of the beam. Additionally, $m_{\text{meas}} = 0.1$ kg for each of the five measurement points is considered in the load vector $\boldsymbol{p}_{\text{own}}$ and in the mass matrix $\boldsymbol{M}$. As usual, the Rayleigh damping matrix $\boldsymbol{C} = \alpha(\xi)\boldsymbol{M} + \beta(\xi)\boldsymbol{K}$ is used to consider damping effects. The Newmark method [36] is applied for solving the differential equation system using the time steps $k = \{0, 1, \ldots, k_{\text{max}}\}$ and the time increment $\Delta t = 1/f_{\text{s}}$ (resulting from the sampling frequency of $f_{\text{s}} = 204.8$ Hz in the conducted measurements).

For the EnKF, the initial state is quantified using normal distributions with a coefficient of variation of 10 %, which is equal to that in Section 3.1. The ensemble size is set to $q = 100$. The model noise terms are defined equally to Section 3.1 ($\boldsymbol{w}_k$ for each degree of freedom) as

$$\begin{aligned} \boldsymbol{w}_k = \begin{pmatrix} w_{u_k} \\ w_{\dot{u}_k} \end{pmatrix} &\sim \begin{pmatrix} \mathcal{N}\left(0, \left(0.01 \cdot \mu_{u_k}\right)^2\right) \\ \mathcal{N}\left(0, \left(0.01 \cdot \mu_{\dot{u}_k}\right)^2\right) \end{pmatrix} \quad \text{and} \\ w_{E_k} &\sim \mathcal{N}\left(0, \left(0.001 \cdot \mu_{E_k}\right)^2\right). \end{aligned} \tag{29}$$

Observations of vertical accelerations a_y are synthetically produced (Section 3.2.1) or measured using the MEDA measurement system on the structure (Section 3.2.2) at five locations; see Figure 11 (top).

3.2.1. Synthetic Measurement Data

The measurement noise is presumed to be small. To show the influence of the measurement noise on the system state and the parameter estimation, three different values are chosen here:

$$\begin{aligned} v_k &\sim \mathcal{N}\left(0, \sigma_{v_k}^2\right) \qquad \text{with} \\ \sigma_{v_k} &= \{0.001, 0.01, 0.1\}. \end{aligned} \tag{30}$$

The parameters E_{real} = 200,000 MN/m^2 and $\xi_{\text{real}} = 0.17$ % are chosen as the reference in each case. The most important results with synthetic measurement data are displayed in Figures 12 and 13.

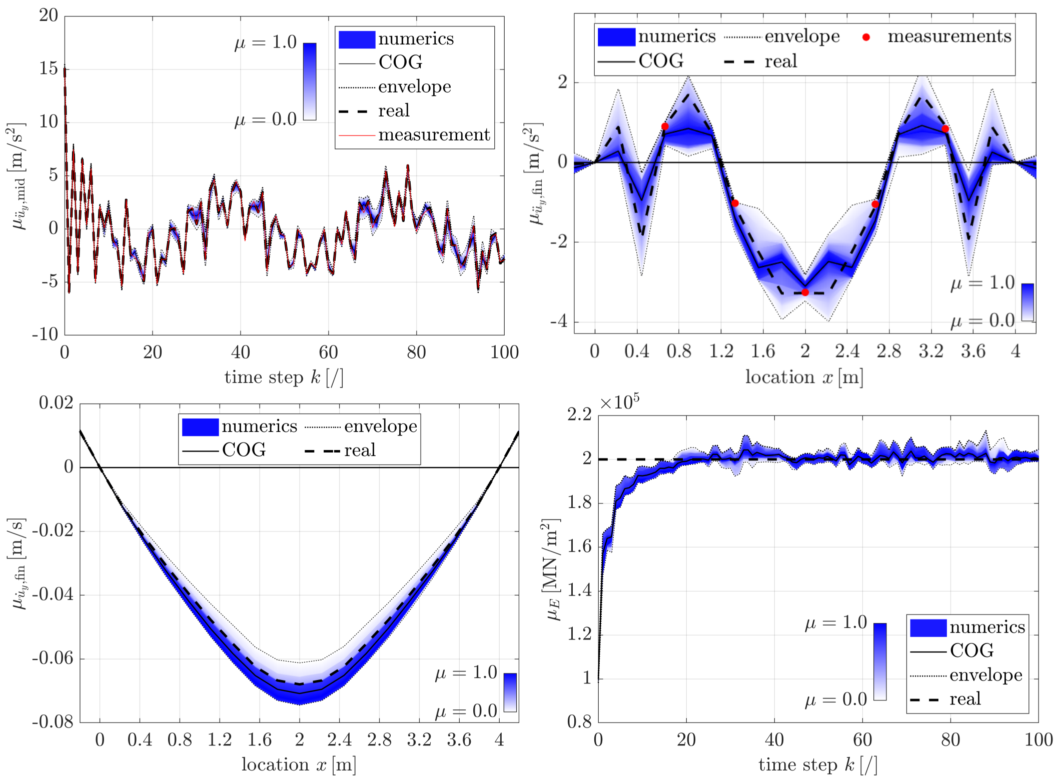

Figure 12. Results with synthetic measurement data with $\sigma_{v_k} = 0.01$: (**top left**): mean of vertical acceleration in the beam center $\mu_{\ddot{u}_y}(2,t)$, (**top right**): mean of final vertical acceleration $\mu_{\ddot{u}_y}(x,100)$, (**bottom left**): mean of final vertical velocity $\mu_{\dot{u}_y}(x,100)$, (**bottom right**): mean of Young's modulus $\mu_E(t)$.

The measurement data are almost equal to the real data in Figure 12 (top left), since the measurement noise is small. The fuzzy-valued mean of the vertical acceleration in the beam center is estimated with only small deviations. The real vertical acceleration is enveloped by the numerical results, and the COG curve is close to the real data; see Figure 12 (top right) for the final system state. The vertical velocity is also estimated very well due to the fact that $\dot{\boldsymbol{u}}_0 = \boldsymbol{0}$ (see Equation (28)) over the beam length, an example of which is shown in Figure 12 (bottom left) for the final system state. The deviation between the real vertical velocity and the COG curve of the numerics results from the symmetric triangular fuzzy number for $\tilde{\xi}$ with the core value of 0.5 % instead of the real value $\xi_{\mathrm{real}} = 0.17$ %. Nevertheless, the real vertical velocity is also enveloped by the numerical values. The mean value of Young's modulus is depicted in Figure 12 (bottom right). The real value E_{real} = 200,000 MN/m^2 is found very quickly with slight variations above and below it. The variations in the model parameter estimation due to the model and the measurement noise are increased due to the present uncertainty in the damping ratio $\tilde{\xi}$. However, the estimation is not adversely influenced by the consideration of the fuzzy-valued parameter.

The results are naturally influenced by all selected numerical parameters. In the following, the variation in the measurement noise is investigated, leading to the results in Figure 13. The prediction of the acceleration in the middle of the beam $\mu_{\ddot{u}_y}(2,t)$ is more noisy for higher measurement noise σ_{v_k} and vice versa (Figure 13 (top left/top right)). Furthermore, it can be seen that the real value of Young's modulus E_{real} is reached much more slowly the higher the noise is (Figure 13 (bottom left/bottom right)). Note that in the case of the smallest measurement noise $\sigma_{v_k} = 0.01$, the scatter in $\mu_E(t)$ is almost the same as in Figure 12 (bottom right) due to the unchanged parameter noise w_{E_k}. The highest measurement noise $\sigma_{v_k} = 0.1$ leads to the weakest update for the Kalman gain, since the measurement data are less trustworthy. Thus, the discrepancy between the model results and the measurement data is weighted less. In general, appropriate values for the measurement and the model noise have to be chosen by the user.

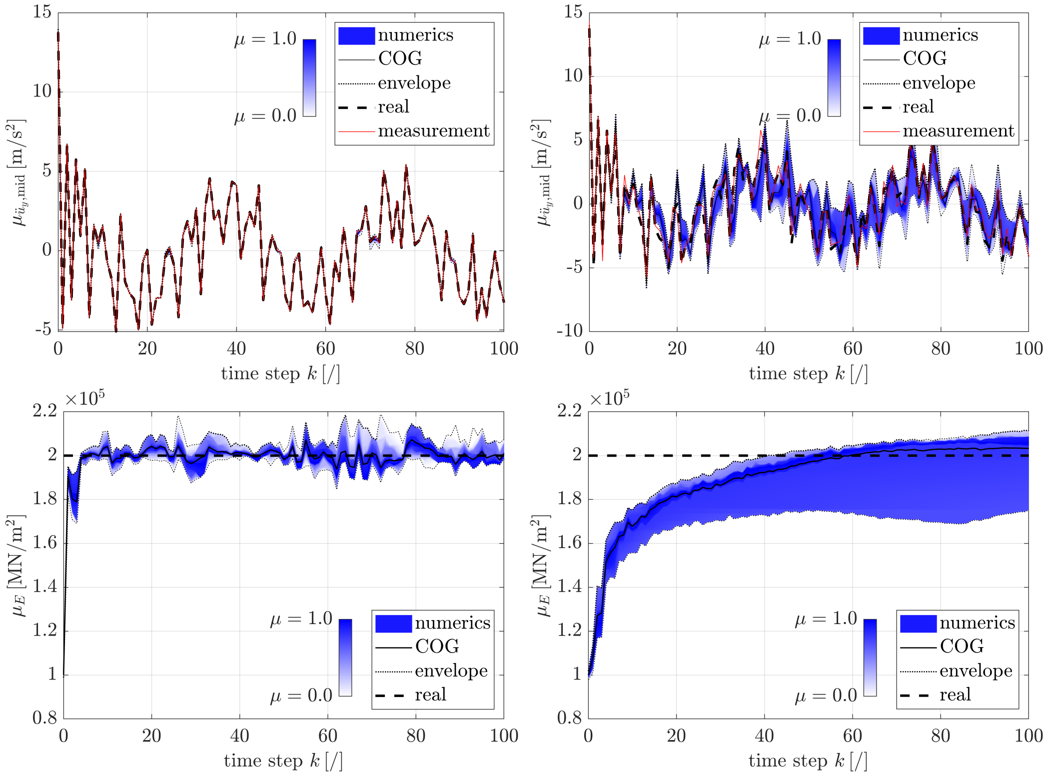

Figure 13. Selected results obtained with higher and smaller measurement noise: (**top left**): mean of vertical acceleration in the beam center $\mu_{\ddot{u}_y}(2,t)$ with $\sigma_{v_k} = 0.001$, (**top right**): mean of vertical acceleration in the beam center $\mu_{\ddot{u}_y}(2,t)$ with $\sigma_{v_k} = 0.1$, (**bottom left**): mean of Young's modulus $\mu_E(t)$ with $\sigma_{v_k} = 0.001$, (**bottom right**): mean of Young's modulus $\mu_E(t)$ with $\sigma_{v_k} = 0.1$.

3.2.2. Real Measurement Data

The measurement noise was determined as the difference between the recorded and the filtered measurement data in this section. A lowpass filter was applied with a passband frequency of 50 Hz. The covariance matrix $\boldsymbol{R}$ of the measurement noise was then determined as

$$\boldsymbol{R} = 10^{-4} \cdot \begin{pmatrix} 0.6990 & 0 & 0 & 0 & 0 \\ & 0.3753 & 0 & 0 & 0 \\ & & 0.9798 & 0 & 0 \\ & & & 0.5983 & 0 \\ \text{sym.} & & & & 0.8534 \end{pmatrix} \tag{31}$$

with a maximum standard deviation value $\max(\sigma_v) = \sqrt{10^{-4} \cdot 0.9798} \approx 0.01$, equivalent to the measurement noise value in Section 3.2.1.

The results of the selected system state variables and Young's modulus as the model parameter to be estimated are shown in Figure 14. A total of 1000 time steps were used, leading to a total time of $t_{\text{tot}} \approx 4.88$ s.

In the case of real measurement data, the vertical acceleration in the beam center is also predicted well despite the presence of an uncertain, fuzzy-valued damping ratio. The real curve, the measurement curve, and the numerical prediction curve of the vertical acceleration in the beam center are qualitatively and quantitatively similar; see Figure 14 (top left). For the final state, the vertical acceleration is predicted very well (Figure 14 (top right)), whereas quantitative deviations are present for the vertical velocity (Figure 14 (bottom left)) with a maximum of 15 % between the real curve and the COG curve. The mean of

Young's modulus is depicted in Figure 14 (bottom right). Transient effects are present in the conducted measurement and visible in the recorded acceleration data but are decaying after approximately 2 s (400 timesteps). The estimation of the real value E_{real} = 200,000 MN/m^2 has been performed successfully.

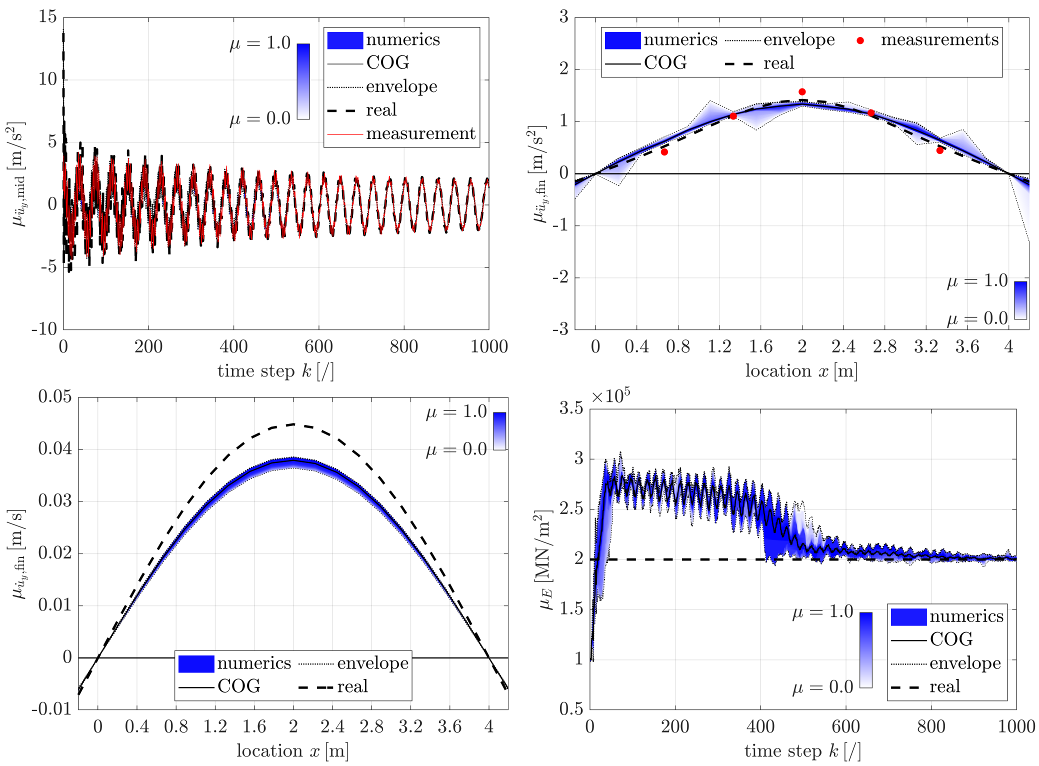

Figure 14. Results with real measurement data: (**top left**): mean of vertical acceleration in the beam center $\mu_{\ddot{u}_y}(2,t)$; (**top right**): mean of final vertical acceleration $\mu_{\ddot{u}_y}(x,1000)$, (**bottom left**): mean of final vertical velocity $\mu_{\dot{u}_y}(x,1000)$; (**bottom right**): mean of Young's modulus $\mu_E(t)$.

4. Discussion and Conclusions

The improvement in the prediction quality through the use of numerical simulation and measurement can be achieved through the data assimilation of the both. In the case of uncertainties influencing the numerical prediction, the classification of aleatory and epistemic uncertainties and the definition of a multilayered uncertainty space are proposed in this contribution. The obtained numerical results have been compared with the observations of system state variables, using either synthetic or real measurement data. Furthermore, the ensemble Kalman filter (EnKF) used has been extended to simultaneously estimate an unknown model parameter. It has been shown using an academic example that the application of non-stochastic uncertainty models is useful for present uncertain variables if no exact probability density functions are known. Thus, a reasonable numerical prediction can be achieved. The overall testing of the proposed integration of the data-assimilation approach in a multilayered uncertainty space can be considered as successful, also for an MDOF laboratory structure, even if some quantitative deviations in results are still present.

Besides this general conclusion, some specific conclusions can also be made as follows. Uncertainties can be present either in initial conditions or in system parameters. In the academic example, the influence of uncertain initial conditions on the system state estimation was small and disappeared after a limited number of time steps. It is important to mention that it is necessary for a successful estimation using the EnKF that the uncertain initial conditions are close to the real values and that the model noise is large enough to enable assimilation in consideration of the observations. Furthermore, the extension to an interval-stochastic mean value of the initial conditions has been investigated. The system state and model parameter estimation is successful, but higher computational costs are unavoidable. In the presented example, the definition of non-stochastic initial conditions is not beneficial.

It has been demonstrated that uncertain model parameters lead to a more continuous influence on the estimations since they are present at each time step in contrast to the initial conditions. Bad or useless estimations appear if wrong probability density functions are assumed. Even though non-stochastic uncertainty models lead to non-stochastic outcomes during data assimilation, the real values can be captured in the case of properly defined input variables. Fuzzy-valued input parameters extend the concept of intervals through a membership function with a higher informative value at the expense of higher computational costs.

The applicability of a multilayered uncertainty space is finally shown on a MDOF example, independently of synthetic or real measurement data. The system state and the model parameter estimation were successfully conducted for both cases.

For future studies, the following aspects can be considered to improve or to extend the presented approach. Localization effects [39,40] would improve the numerical prediction for a MDOF structure by separating the effects of different observations. Although the EnKF has successfully been applied in this contribution, other Kalman filters can alternatively be used as well, since the proposal of a multilayered uncertainty space is independent of the used filter. In the framework of structural health monitoring, the presented approach can also be used for the detection of system changes such as stiffness reduction due to damage.

Author Contributions: Conceptualization, M.D.; methodology, M.D.; software, M.D. and C.H.; validation, M.D.; formal analysis, M.D. and C.H.; investigation, M.D. and C.H.; data curation, C.H.; writing—original draft preparation, M.D. and C.H.; writing—review and editing, M.D. and Y.P.; project administration, Y.P.; funding acquisition, Y.P. All authors have read and agreed to the published version of the manuscript.

Funding: The authors acknowledge support by the German Research Foundation and the Open Access Publication Fund of TU Berlin. Furthermore, the authors gratefully acknowledge the financial support of the German Research Foundation within the Subproject 4 (312928137) of the Priority Programme "Polymorphic uncertainty modelling for the numerical design of structures–SPP 1886".

Institutional Review Board Statement: Not applicable.

Informed Consent Statement: Not applicable.

Data Availability Statement: The data presented in this study are available on request from the corresponding author. The data are not publicly available.

Conflicts of Interest: The authors declare no conflict of interest.

Abbreviations

The following abbreviations are used in this manuscript:

CDF	cumulative distribution function
COG	center of gravity
EnKF	ensemble Kalman filter
EnSRF	ensemble square root filter
MDOF	multi-degree-of-freedom
PDF	probability density function
POD	proper orthogonal decomposition
RRSQRT	reduced rank square root Kalman filter
UKF	unscented Kalman filter

References

1. Pu, Z.; Kalnay, E. Numerical Weather Prediction Basics: Models, Numerical Methods, and Data Assimilation. In *Handbook of Hydrometeorological Ensemble Forecasting*; Duan, Q., Pappenberger, F., Thielen, J., Wood, A., Cloke, H.L., Schaake, J.C., Eds.; Springer: Berlin/Heidelberg, Germany, 2018; pp. 1–31. [CrossRef]
2. Urrea, C.; Agramonte, R.; Diraco, G. Kalman Filter: Historical Overview and Review of Its Use in Robotics 60 Years after Its Creation. *J. Sens.* **2021**, *2021*, 9674015. [CrossRef]
3. Pasricha, G.K. Kalman filter and its economic applications. *Munich Pers. RePEc Arch.* **2006**, 22734.
4. Auger, F.; Hilairet, M.; Guerrero, J.M.; Monmasson, E.; Orlowska-Kowalska, T.; Katsura, S. Industrial Applications of the Kalman Filter: A Review. *IEEE Trans. Ind. Electron.* **2013**, *60*, 5458–5471. [CrossRef]
5. Kálmán, R.E. A New Approach to Linear Filtering and Prediction Problems. *J. Basic Eng.* **1960**, *82*, 35–45. [CrossRef]
6. Burgers, G.; van Leeuwen, P.J.; Evensen, G. Analysis Scheme in the Ensemble Kalman Filter. *Mon. Weather. Rev.* **1998**, *126*, 1719–1724. [CrossRef]
7. Gillijns, S.; Mendoza, O.; Chandrasekar, J.; De Moor, B.; Bernstein, D.; Ridley, A. What is the ensemble Kalman filter and how well does it work? In Proceedings of the 2006 American Control Conference, Minneapolis, MN, USA, 14–16 June 2006; pp. 4448–4453. [CrossRef]
8. Whitaker, J.S.; Hamill, T.M. Ensemble Data Assimilation without Perturbed Observations. *Mon. Weather. Rev.* **2002**, *130*, 1913–1924. [CrossRef]
9. Tippett, M.K.; Anderson, J.L.; Bishop, C.H.; Hamill, T.M.; Whitaker, J.S. Ensemble Square Root Filters. *Mon. Weather. Rev.* **2003**, *131*, 1485–1490. [CrossRef]
10. Treebushny, D.; Madsen, H. A New Reduced Rank Square Root Kalman Filter for Data Assimilation in Mathematical Models. In Proceedings of the Computational Science—ICCS 2003, St. Petersburg, Russia, 2–4 June 2003; Sloot, P.M.A., Abramson, D., Bogdanov, A.V., Dongarra, J.J., Zomaya, A.Y., Gorbachev, Y.E., Eds.; Springer: Berlin/Heidelberg, Germany, 2003; pp. 482–491. [CrossRef]
11. Treebushny, D.; Madsen, H. On the construction of a reduced rank square-root Kalman filter for efficient uncertainty propagation. *Future Gener. Comput. Syst.* **2005**, *21*, 1047–1055. [CrossRef]
12. Wan, E.; van der Merwe, R.; Nelson, A. Dual Estimation and the Unscented Transformation. *Adv. Neural Inf. Process.* **1999**, *12*, 666–672.
13. Wan, E.; Van der Merwe, R. The unscented Kalman filter for nonlinear estimation. In Proceedings of the IEEE 2000 Adaptive Systems for Signal Processing, Communications, and Control Symposium (Cat. No.00EX373), Lake Louise, AB, Canada, 4 October 2000; pp. 153–158. [CrossRef]
14. Van der Merwe, R.; Wan, E. The square-root unscented Kalman filter for state and parameter-estimation. In Proceedings of the 2001 IEEE International Conference on Acoustics, Speech, and Signal Processing (Cat. No.01CH37221), Salt Lake City, UT, USA, 7–11 May 2001; Volume 6, pp. 3461–3464. [CrossRef]
15. Fletcher, S.J. *Data Assimilation for the Geosciences: From Theory to Application*; Elsevier: Amsterdam, The Netherlands, 2017. [CrossRef]
16. Campestrini, C.; Heil, T.; Kosch, S.; Jossen, A. A comparative study and review of different Kalman filters by applying an enhanced validation method. *J. Energy Storage* **2016**, *8*, 142–159. [CrossRef]
17. Kim, S.; Deshpande, V.M.; Bhattacharya, R. Robust Kalman Filtering With Probabilistic Uncertainty in System Parameters. *IEEE Control. Syst. Lett.* **2021**, *5*, 295–300. [CrossRef]
18. Chui, C.K.; Chen, G. Kalman filtering for interval systems. In *Kalman Filtering: With Real-Time Applications*; Springer: Berlin/Heidelberg, Germany, 2009; Chapter 10, pp. 143–163. [CrossRef]
19. Chen, G.; Wang, J.; Shieh, L. Interval Kalman filtering. *IEEE Trans. Aerosp. Electron. Syst.* **1997**, *33*, 250–259. [CrossRef]
20. Matía, F.; Jiménez, A.; Al-Hadithi, B.M.; Rodríguez-Losada, D.; Galán, R. The fuzzy Kalman filter: State estimation using possibilistic techniques. *Fuzzy Sets Syst.* **2006**, *157*, 2145–2170. [CrossRef]
21. Matía, F.; Jiménez, V.; Alvarado, B.P.; Haber, R. The fuzzy Kalman filter: Improving its implementation by reformulating uncertainty representation. *Fuzzy Sets Syst.* **2021**, *402*, 78–104. [CrossRef]
22. Jiménez, V.; Alvarado, B.P.; Matía, F. A set of practical experiments to validate the fuzzy Kalman filter. *Fuzzy Sets Syst.* **2021**, *417*, 152–170. [CrossRef]
23. Kiureghian, A.D.; Ditlevsen, O. Aleatory or epistemic? Does it matter? *Struct. Saf.* **2009**, *31*, 105–112. [CrossRef]
24. Evensen, G. Sequential data assimilation with a nonlinear quasi-geostrophic model using Monte Carlo methods to forecast error statistics. *J. Geophys. Res. Ocean.* **1994**, *99*, 10143–10162. [CrossRef]
25. Evensen, G. Advanced Data Assimilation for Strongly Nonlinear Dynamics. *Mon. Weather. Rev.* **1997**, *125*, 1342–1354. [CrossRef]
26. Evensen, G. The ensemble Kalman filter for combined state and parameter estimation. *IEEE Control. Syst. Mag.* **2009**, *29*, 83–104. [CrossRef]
27. Yang, X.; Delsole, T. Using the ensemble Kalman filter to estimate multiplicative model parameters. *Tellus A* **2009**, *61*, 601–609. [CrossRef]
28. Narasingam, A.; Siddhamshetty, P.; Kwon, J.S.I. Handling Spatial Heterogeneity in Reservoir Parameters Using Proper Orthogonal Decomposition Based Ensemble Kalman Filter for Model-Based Feedback Control of Hydraulic Fracturing. *Ind. Eng. Chem. Res.* **2018**, *57*, 3977–3989. [CrossRef]

29. Mendoza, O.B. Data Assimilation in Magnetohydrodynamics Systems Using Kalman Filtering. Ph.D. Thesis, Katholieke Universiteit Leuven (KU Leuven), Leuven, Belgium, 2005.
30. Papaioannou, I.; Daub, M.; Drieschner, M.; Duddeck, F.; Ehre, M.; Eichner, L.; Eigel, M.; Götz, M.; Graf, W.; Grasedyck, L.; et al. Assessment and design of an engineering structure with polymorphic uncertainty quantification. *GAMM-Mitteilungen* **2019**, *42*, e201900009. [CrossRef]
31. Hanss, M. *Applied Fuzzy Arithmetic: An Introduction with Engineering Applications*, 1st ed.; Springer: Berlin/Heidelberg, Germany, 2005. [CrossRef]
32. Möller, B.; Beer, M. *Fuzzy Randomness-Uncertainty in Civil Engineering and Computational Mechanics*; Springer: Berlin/Heidelberg, Germany, 2004. [CrossRef]
33. Freitag, S.; Edler, P.; Kremer, K.; Meschke, G. Surrogate modelling for solving optimization problems with polymorphic uncertain data. In Proceedings of the 8th International Workshop on Reliable Engineering Computing (REC 2018), Liverpool, UK, 16–18 July 2018; pp. 31–39.
34. Götz, M.; Graf, W.; Kaliske, M. Structural design with polymorphic uncertainty models. *Int. J. Reliab. Saf.* **2015**, *9*, 112–131. [CrossRef]
35. Drieschner, M.; Eichner, L.; Seiffarth, F.; Petryna, Y. PolyUQ: Framework for Solving Problems with Polymorphic Uncertainties. Preprint Technische Universität Berlin. Available online: https://depositonce.tu-berlin.de/items/dd13e961-1d3f-405d-a720-ad77bd795ad2 (accessed on 15 October 2023).
36. Newmark, N.M. A Method of Computation for Structural Dynamics. *J. Eng. Mech. Div.* **1959**, *85*, 67–94. [CrossRef]
37. Dong, W.; Shah, H.C. Vertex method for computing functions of fuzzy variables. *Fuzzy Sets Syst.* **1987**, *24*, 65–78. [CrossRef]
38. Leekwijck, W.V.; Kerre, E.E. Defuzzification: Criteria and classification. *Fuzzy Sets Syst.* **1999**, *108*, 159–178. [CrossRef]
39. Hamill, T.M.; Whitaker, J.S.; Snyder, C. Distance-Dependent Filtering of Background Error Covariance Estimates in an Ensemble Kalman Filter. *Mon. Weather. Rev.* **2001**, *129*, 2776–2790. [CrossRef]
40. Petrie, R.E. Localization in the Ensemble Kalman Filter. Ph.D. Thesis, University of Reading, Reading, UK, 2008.